Defect-tolerant extreme ultraviolet nanoscale printing

L. Urbanski,[1,*] A. Isoyan,[2] A. Stein,[3] J. J. Rocca,[1] C. S. Menoni,[1] and M. C. Marconi[1]

[1]*Engineering Research Center for Extreme Ultraviolet Science and Technology, and Electrical and Computer Engineering Department, Colorado State University, Fort Collins, Colorado 80523, USA*

[2]*Synopsys Inc., Hillsboro, Oregon 97124, USA*

[3]*Center for Functional Nanomaterials, Brookhaven National Laboratory, Upton, New York 11973-5000, USA*

**Corresponding author: urbanski@engr.colostate.edu*

Received April 30, 2012; revised July 10, 2012; accepted July 11, 2012;
posted July 11, 2012 (Doc. ID 167605); published August 27, 2012

We present a defect-free lithography method for printing periodic features with nanoscale resolution using coherent extreme ultraviolet light. This technique is based on the self-imaging effect known as the Talbot effect, which is produced when coherent light is diffracted by a periodic mask. We present a numerical simulation and an experimental verification of the method with a compact extreme ultraviolet laser. Furthermore, we explore the extent of defect tolerance by testing masks with different defect layouts. The experimental results are in good agreement with theoretical calculations.

OCIS codes: 140.7240, 340.7480, 110.4235.

We describe a defect-free lithography technique based on the Talbot effect that uses extreme ultraviolet (EUV) laser light to print nanoscale features. A periodic diffractive object referred further in the text as to the mask was illuminated by coherent EUV light to create self-images that were printed on a photoresist coated sample. This self-imaging method renders error-free prints despite the existence of defects in the mask.

The working principle of this technique relies on the effect of self-imaging discovered by Talbot in the 19th century [1]. Periodic structures illuminated by coherent light create self-images at planes, called Talbot planes, located at distances determined by the periodicity of the mask and the wavelength of the illumination, as schematically represented in Figure 1.

Talbot coherent lithography has been used at longer wavelengths to pattern photonic crystals using a mask composed of an array of holes in what was defined as coherent diffraction lithography [2]. Recently, a generalization of the Talbot effect was demonstrated by Isoyan, *et al.* [3], in an experiment where the mask was composed of an array of cells of arbitrary motifs tilled periodically in a square matrix. This method of patterning, which was called generalized Talbot imaging (GTI), allowed the printing of faithful replicas of the mask up to the sixth Talbot plane using EUV illumination.

One interesting characteristic of the Talbot effect for lithography applications is its capability to produce defect-free prints from faulty masks. Dammann, *et al.* [4] showed that defective periodic masks produce self-images without an apparent defect. In the experiment described in [4] the defect was in the form of a thin scratch over a periodic mask and the illumination source was in the visible range, which limits the minimum size of the printed features. In this work, we investigate the defect tolerance of the self-imaging method applied to printing periodic nanostructures using EUV radiation. Different defect densities were introduced in a periodic mask that illuminated with coherent EUV light rendered defect-free prints. Furthermore, we present numerical simulation of self-images that are in good agreement with the experimental results.

The most convenient way to describe the GTI effect is using the spatial frequency domain. A derivation similar to the one presented by Lohman [5] yields a final expression of the amplitude in the Talbot plane given by:

$$\begin{aligned} U_{\mathrm{TOT}}(x,z) &= D(x,z) + A_0 \\ &\quad + \sum_{m\neq 0} A_m \exp\left[-2i\pi\left(m\nu_0 x - m^2\frac{z}{z_T}\right)\right] \\ &= D(x,z) + U(x, z + Nz_T), \end{aligned} \tag{1}$$

where $U_{\mathrm{TOT}}(x,z)$ is the total light amplitude at the Talbot plane, $D(x,z)$ is the intensity due to the presence of the defect, A_0 is a constant background illumination, A_m is the m-th Fourier coefficient of the periodic transmission mask, $\nu_0 = \frac{1}{p}$ is the spatial frequency defined as the inverse of mask's period, and z_T is the Talbot distance. For simplicity, in Eq. (1) only one transverse coordinate was included, but this expression can be easily expanded to the two-dimensional periodicity in the transverse plane by adding a similar functional relationship for the y coordinate.

The propagation of the beam is along the z axis. Equation (1) addresses the question of defect tolerance twofold. First, a localized (non-periodic) defect in the mask does not have periodic character along the axis of propagation; thus, it will not produce a self-image. Second,

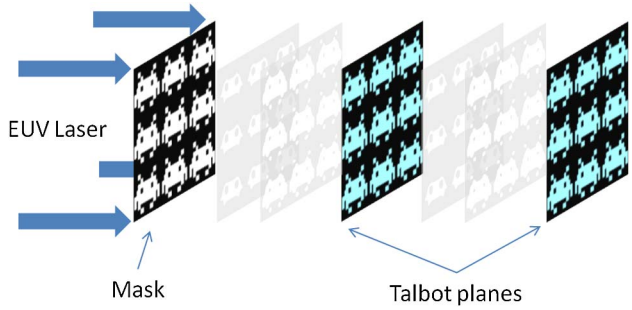

Fig. 1. (Color online) Experimental setup. The EUV laser illuminates the Talbot mask that renders self-images at the Talbot planes where the sample is located.

the contribution from the defect to the final image is an additive term that depends on the characteristics of the defect itself.

To properly evaluate $D(x, y)$ in Eq. (1), it is necessary to know the defect's size and spectral spatial components. As a first approximation, the defect can be considered as background illumination whose intensity depends on the relative area of the defect to the total area of the mask. If this ratio is small, the contribution of the defect to the final image is small and, as a consequence, this results in excluding the defect at the reconstruction plane. This fact is of particular significance when the self-imaging effect is used in a lithography set up because it leads to defect-tolerant printing. Figure 2 shows a graphical demonstration of this characteristic. Figure 2(a) is an array of unit cells with an arbitrary design. For this graphical demonstration, we chose the profile of creatures from the classic video game, Space Invaders. The defect had a form of a different kind of invader, and was located at the center of the mask. The mask was composed of 10,000 unit cells arranged in a square matrix. Figure 2(b) is the numerical reconstruction of the mask shown in Figure 2(a), calculated by means of Fresnel-Kirchhoff diffraction integral.

To verify the concept of defect tolerance in the GTI, we did an experiment using a compact EUV laser. A schematic of the experimental setup is shown in Fig. 1. The components of the setup are the EUV laser used for coherent illumination, the periodic Talbot mask, and the sample that was placed at the first Talbot plane.

The light source used in this experiment is a compact $\lambda = 46.9$ nm capillary discharge EUV laser. This laser is well suited to coherent printing because it provides both temporally and spatially coherent light of average energy per pulse of 0.1 mJ [6]. The spectral bandwidth of the laser pulses is approximately $\Delta\lambda/\lambda = 3.5 \times 10^{-5}$, yielding a coherence length of the order of 750 μm [7]. The spatial coherence radius is approximately 550 μm at the distance where the exposure took place [8]. The mask was defined in a thin layer of photoresist deposited on a thin Si_3N_4 membrane. The details of the mask fabrication are described in [3]. The primitive cell size was 5×5 μm^2, resulting in a Talbot distance of 1 mm for the 46.9 nm wavelength of the illumination. The defects were planted by substituting the native motif by a completely different one, called the impostor cell. Downstream from the mask, a silicon wafer coated with a photoresist was placed to capture the self-image of the mask. The recording medium was a 100 nm layer of poly-methyl-methacrylate (PMMA) resist. The distance between the mask and the sample planes was set to the first Talbot distance.

To investigate the extent of defect tolerance, two different arrangements of defects were applied. A single impostor cell was planted in the middle of the mask, yielding the size ratio of the defect to the entire mask of 0.01%. In the second case, an entire row of native cells was replaced by a row consisting of impostor motif yielding the defect to mask area ratio of 1%. The electron microscope scans of the masks with different defect layouts are shown in Figs. 3(a) and 3(b).

The mask was illuminated with 300 laser pulses at a rate of 1 Hz. The exposure time can be reduced increasing the repetition rate of the laser to 4 Hz [9]. After the exposure, the resist was developed and inspected with an atomic force microscope (AFM). The AFM scans of the prints in the sample are illustrated in Figs. 3(c) and 3(d). Both scans are 20×20 μm^2 in size. The scans cover the region where the defects were placed in the Talbot mask; however, these defects do not appear in the prints.

The resolution of the diffraction limited image depends on the characteristics of the mask that determines the numerical aperture of the optical system. The image resolution is given by:

$$\Delta \approx \frac{\lambda}{2}\sqrt{1 + \frac{2np^2}{\lambda W}}, \tag{2}$$

where, n is the Talbot order and W is the mask's size.

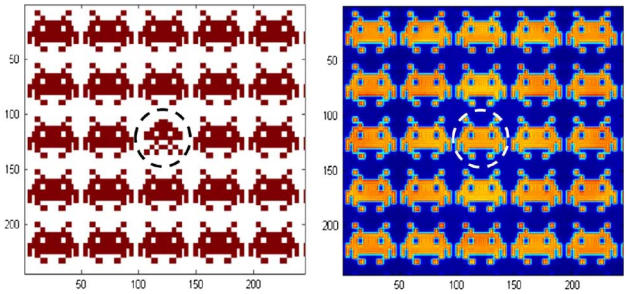

Fig. 2. (Color online) Numerical simulation of the defect-tolerance concept of the GTI for a mask composed of 10,000 cells. (a) Mask with a defect. (b) Intensity distribution at the Talbot plane. The reconstruction does not show the defect indicated in the dashed lined circle.

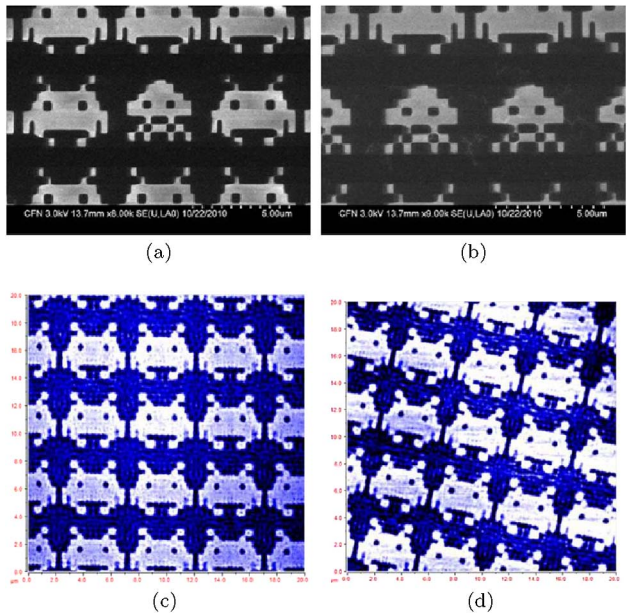

Fig. 3. (Color online) Electron microscope scans of the two Talbot masks used in the experiment with on-purpose fabricated defects. (a) Defect equivalent to a single unit cell. (b) Defect equivalent to an entire row of cells. (c) Corresponding AFM scans of the reconstruction at first Talbot plane corresponding to a mask with a single cell defect. (d) A mask with entire row of defects.

The ultimate resolution in the printing, however, is largely influenced by the response of the photoresist, the coherence of the illumination, the spatial spectral composition of the motif of the unit cell, and the periodicity of the cells. The density and the distribution of the defects in the mask also will influence the final resolution of the print. The non-linear response of the photoresist, for example, can improve the resolution of the print as compared with the resolution of the self-image. On the other hand, if the defect has some periodicity, it may have a detrimental effect on the final print. In summary, the resolution of the print depends on the characteristics of each specific mask and defect distribution. A detailed study of the final resolution of the print is beyond the scope of this work.

In conclusion, we have demonstrated a defect-tolerant EUV lithography technique. The experimental results are in good agreement with both analytical and numerical theoretical considerations. Two different densities of defects were investigated: a single cell (defect to mask ratio of 0.01% in area) and an entire row of cells (defect to mask ratio of 1% in area). It is important to notice that these two defect densities are orders of magnitude larger than the typical acceptable defect count in a lithography mask. In both cases, however, no sign of defect in the print was observed. We envision that the presented technique could be used to consistently print error-free periodic structures such as calibration gratings for scanning microscopes or photonic crystal structures. The availability of highly coherent EUV compact sources in conjunction with the classical Talbot imaging effect offer an opportunity to implement an alternative nanoscale printing method for periodic structures that is immune to the presence of defects in the mask [10].

This work was supported by the National Science Foundation, award ECCS 0901806 and the NSF Engineering Research Center for Extreme Ultraviolet Science and Technology, award EEC 0310717. The masks were fabricated at the Center for Functional Nanomaterials, Brookhaven National Laboratory, which is supported by the U.S. Dept. of Energy, Office of Basic Energy Sciences, under Contract No. DE-AC02-98CH10886.

References

1. H. Talbot, Philos. Mag. **9**, 401 (1836).
2. C. Zanke, M. Qi, and H. I. Smith, J. Vac. Sci. Technol. B **22**, 3352 (2004).
3. A. Isoyan, F. Jiang, Y. C. Cheng, F. Cerrina, P. Wachulak, L. Urbanski, J. J. Rocca, C. S. Menoni, and M. C. Marconi, J. Vac. Sci. Technol. B **27**, 2931 (2009).
4. H. Dammann, G. Groh, and M. Kock, Appl. Opt. **10**, 1454 (1971).
5. A. W. Lohmann, H. Knuppertz, and J. Jahns, J. Opt. Soc. Am. A **22**, 1500 (2005).
6. B. R. Benware, C. D. Macchietto, C. H. Moreno, and J. J. Rocca, Phys. Rev. Lett. **81**, 5804 (1998).
7. L. Urbanski, M. C. Marconi, L. M. Meng, M. Berrill, O. Guilbaud, A. Klisnick, and J. J. Rocca, Phys. Rev. A **85**, 033837 (2012).
8. Y. Liu, M. Seminario, F. Tomasel, C. Chang, J. J. Rocca, and D. Attwood, Phys. Rev. A **63**, 1 (2001).
9. C. D. Macchietto, B. R. Benware, and J. J. Rocca, Opt. Lett. **24**, 1115 (1999).
10. D. Alessi, D. H. Martz, Y. Wang, M. Berrill, B. M. Luther, and J. J. Rocca, Opt. Lett. **35**, 414 (2010).